Supplementary Information (SI) for Journal of Materials Chemistry A.

Supplementary Information

A Thermomechanically Stable Nanofiber Separator with Multiscale MOF Networks towards High-Efficiency Ion Transport

Feifei Lan[a,1], Huijuan Zhao[a,1,*], Yu jiang, Cancan Jin, Guodong Zhao[a,*], Lin Li[a,b,*]

[a] College of Textiles and Clothing, State Key Laboratory of Bio-Fibers and Eco-Textiles, Qingdao University, Qingdao 266071, PR China

[b] Beijing Key Laboratory of Energy Conversion and Storage Materials, College of Chemistry, Beijing Normal University, Beijing 100875, PR China

[*]Corresponding authors:

hjzhao@qdu.edu.cn (H.J. Zhao)

zhaoguodong@qdu.edu.cn (G.D. Zhao)

lilinll@bnu.edu.cn (L. Li)

[1] Both authors contributed equally to the manuscript.

Table of Contents

Section SI. Experimental Section

1.1 Fabrication of PI nanofiber separators

The polyimide (PI) nanofiber separators were prepared by a facile electrospinning method. 4, 4'-Diaminodiphenyl ether (ODA, 98%, Aladdin) powders were first dissolved in *N, N*-Dimethylformamide (DMF, AR, Sinopharm Chemical Reagent) solvent and then stirred for 20 min until the solution became clear and transparent. Subsequently, pyromellitic dianhydride (PMDA, 99%, Aladdin) powders with an equimolar mass with ODA were introduced into the above solution and stirred continuously until it turned pale yellow, thereby forming uniform polyamic acid (PAA) solution with a concentration of 16 wt. %. The obtained PAA sol was directly used for electrospinning with the following determined parameters: a feeding rate of 3.6 mL h^{-1}, a voltage of 20 kV and a tip-collector distance of 15 cm. The as-spun PAA nanofiber separators were transferred into a vacuum oven at 60 °C overnight to remove excess residual solvent. Eventually, the PAA separators were thermal-imidized by a gradient heating at 100 °C for 1 h, 160 °C for 0.5 h, 250 °C for 0.5 h and 300 °C for 0.5 h with a heating rate of 2 °C min^{-1} to yield yellow PI nanofiber separators.

1.2 Fabrication of PI@ZIF-8 nanofiber separators

The surface alkaline etching strategy was performed on the as-prepared PI nanofiber separators through immersed in 1.0 M potassium hydroxide (KOH, 95%, Aladdin) solution for 1 min and then the remnant KOH was thoroughly rinsed with deionized water. Afterward, the etched PI nanofibers were soaked into a mixed solution composed of 0.24 M zinc nitrate hexahydrate ($Zn(NO_3)_2 \cdot 6H_2O$, AR, 99%, Aladdin) within methanol (AR, Sinopharm Chemical Reagent) solvent for 12 h, which followed by that a methanol solution containing 1.92 M 2-methylimidazole (2-MIM, 98%, Aladdin) was added into the above mixture with constant stirring for 12 h. In the above reaction process, the zeolite imidazole framework (ZIF-8) nanounits were *in-situ* self-assembly on the surface of PI substrate to obtain the 3D multiscale MOF networks. Finally, the thermal treatment in nitrogen atmosphere at 250 °C for 1 h was conducted to re-cyclize the cleaved imide rings on PI surface and simultaneously activate the self-assembled MOF networks by removing the residual solvent, achieving the effective construction of PI@ZIF-8 nanofiber separators.

1.3 Material Characterizations

$$Y = \frac{X}{A \times B}$$

The overall morphology and microstructure were investigated by scanning electron microscope (SEM, JSM-6390LV, Japanese electronics Co., Japan). Elemental analysis was performed by Energy Dispersive Xray spectroscope (Oxford Max80, Zeiss Co., Germany). Fourier transform infrared spectroscopy (FTIR) measurements were obtained using Nicolet iS10 (Thermo Fisher Scientific Co., USA). X-ray photoelectron spectroscopy (XPS) analysis was carried out by PHI5000 Versaprobe III spectrometer (ULVAC-PHI Co., Japan). The crystal structure was conducted by X-ray diffraction (XRD) instrument (MiniFlex 600, Rugaku Corporation Co., Japan) at a scanning rate of 10° min^{-1}. The nitrogen (N_2) adsorption/desorption isotherms were measured by using the TriStar-3000 gas adsorption analyzer (Micromeritics Instrument Co., USA). The electrolyte contact angles were determined by Contact Angle Meter (V5, Yunfan Instrument Co., China) with the selected liquid electrolyte. Differential scanning calorimetry (DSC2500, TA Co., USA) was performed to detect the thermal property of separators with temperature range of 25 to 300 °C at a heating rate of 10 °C min^{-1} in N_2 atmosphere. Stress-strain curves were tested by YM-06A monofilament tensile tester (YuanMore Co., China) with a stretching speed of 10 mm min^{-1}. The unit X (cN) of the tested tensile strength values could be converted to Y (MPa) in accordance with equation (1),

(1)

where A (cm) was the width and B (μm) was the thickness of nanofiber separators.

The electrolyte uptakes of separators could be calculated according to the following equation (2),

$$\text{Uptake} = \frac{W_1 - W_0}{W_0} \times 100\% \tag{2}$$

where W_0 (mg) and W_1 (mg) were the separator masses of the initial and after immersed in liquid electrolyte for 24 h, respectively.

1.4 Electrochemical Measurements

CR2032-type coin cells were assembled for electrochemical measurements in an argon-filled glovebox (Universal (2440/750/900), Shanghai Mikrouna Mech Tech Co., Ltd), where both oxygen and water contents were below 0.1 ppm. The electrochemical stability window was tested by linear sweep voltammetry (LSV) with lithium (Li)‖separator‖stainless steel (SS) cells between 2.0 and 6.0 V at a scan rate of 0.1 mV s^{-1} through AMETEK-AMT (PMC-200) electrochemical workstation. Ionic conductivity was determined by electrochemical impedance spectroscopy (EIS) using SS‖separator‖SS cells with a frequency range from 10^5 to 10^{-1} Hz and an amplitude of 10 mV. The bulk resistance (R_0) was obtained by the intercept of EIS curve with the real axis. The ionic conductivity (σ) was then calculated according to the following equation (3),

$$\sigma = \frac{d}{R_0 S}$$

(3)

where d (μm) was the separator thickness and S (cm^2) was the contact area between the separators and SS sheet, respectively. The Li^+ transference number (t_{Li+}) was carried with symmetric Li‖separator‖Li cells by the combination measurement of DC polarization and AC impedance. A DC potential (ΔE=10 mV) was applied for 1000 s to gain the initial and steady currents. Meanwhile, the AC impedance spectra of the same cells were measured before and after polarization. The equation (4) for calculating t_{Li}^+ was as follows,

$$t_{Li^+} = \frac{I_s(\Delta E - I_0 R_0)}{I_0(\Delta E - I_s R_s)}$$

(4)

where R_0 and R_s were respectively the AC impedances before and after polarization, while I_0 and I_s were the initial and steady currents, respectively.

Multi-cycle galvanostatic charge-discharge performances of the assembled batteries were performed on a LAND CT2001A battery testing system at 25 °C. Wherein, the PE separators with a diameter of 19.0 mm and a thickness of 20.0 μm were selected as the control sample. The symmetric Li‖Li cells were cycled using Li foils with a diameter of 15.6 mm under different current densities and Li deposition amounts. The Li‖Cu cells were operated with a cut-off voltage of 1.0 V for every cycle under a current density of 0.5 mA cm^{-2} with an areal capacity of 1.0 mAh cm^{-2}. The Li-metal batteries were studied using $LiFePO_4$ (LFP, 1C=170 mAh g^{-1}) and NCM811 (1C=200 mAh g^{-1}) as cathodes and metallic Li as anodes. The adopted liquid electrolyte was composed of 1.0 M lithium hexafluorophosphate ($LiPF_6$) within the mixtures of ethylene carbonate (EC)/diethyl carbonate (DEC)/ethylmethyl carbonate (EMC) with a volume ratio of 1:1:1. The charge-discharge tests of LFP‖Li cells were carried out in voltage range of 2.5-4.0 V and NCM811‖Li cells were conducted between 2.8 and 4.3 V. To fabricate the cathode materials, the homogeneous slurry of active substances (LFP or NCM811), super P and polyvinylidene fluoride in a mass ratio of 8:1:1 within N-methyl pyrrolidone solvent was casted onto carbon-coated aluminum foil with a spatula followed by vacuum drying for 48 h to competently remove the residual solvent. Specifically, the average areal doping amount of the active materials for the resulting LFP and NCM811 cathodes was qualified to be ~3.0 and ~3.6 mg cm^{-2}, respectively.

1.5 Theoretical calculation methods

All density functional theory (DFT) calculations were carried out in the CP2K code. All calculations employed a mixed Gaussian and planewave basis sets. Core electrons were represented with norm-conserving Goedecker-Teter-Hutter pseudopotentials, and the valence electron wavefunction was expanded in a double-zeta basis set with polarization functions along with an auxiliary plane wave basis set with an energy cutoff of 450 eV. The generalized gradient approximation exchange-correlation functional of Perdew, Burke and Enzerhof (PBE) was applied. Each configuration was optimized through the Broyden-Fletcher-

Goldfarb-Shanno (BGFS) algorithm with SCF convergence criteria of 1.0 × 10^{-5} au. The van der Waals correction of Grimme's DFT-D3 model was also adopted. The Brillouin-zone integration was sampled with a Γ-centered Monkhorst-Pack mesh of 1 × 1 × 1.

The adsorption energy between the adsorbate and the MOFs could be calculated using the following equation (5):

$$\Delta E_{ads} = E_{adsorbate@COF} - E_{MOF} - E_{adsorbate} \tag{5}$$

where $E_{adsorbate@MOF}$ and E_{MOF} represented the total energies of the MOFs with and without the adsorption of adsorbate, respectively. $E_{adsorbate}$ was the total energy of the adsorbate. According to this equation, a negative adsorption energy corresponded to a stable adsorption structure.

Section SII. Supporting Figures and Tables

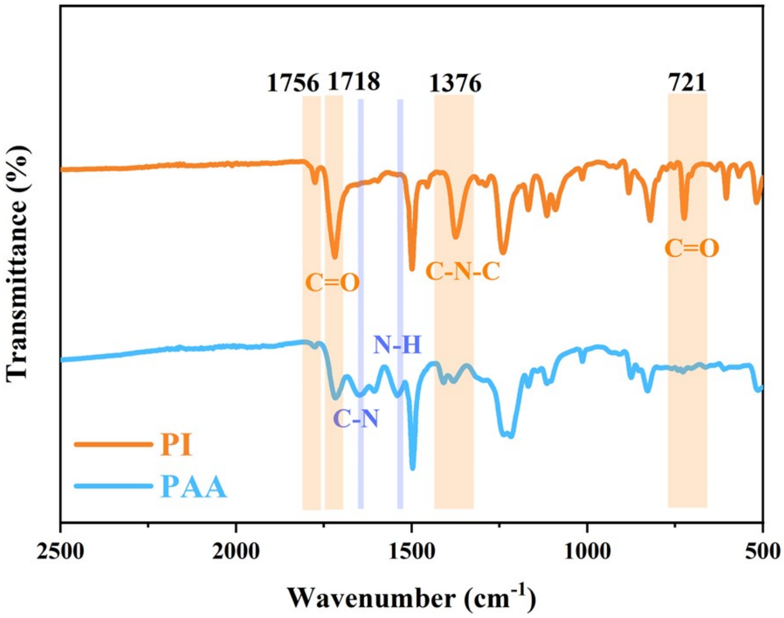

Fig. S1 FTIR spectra of PAA and PI nanofiber separators.

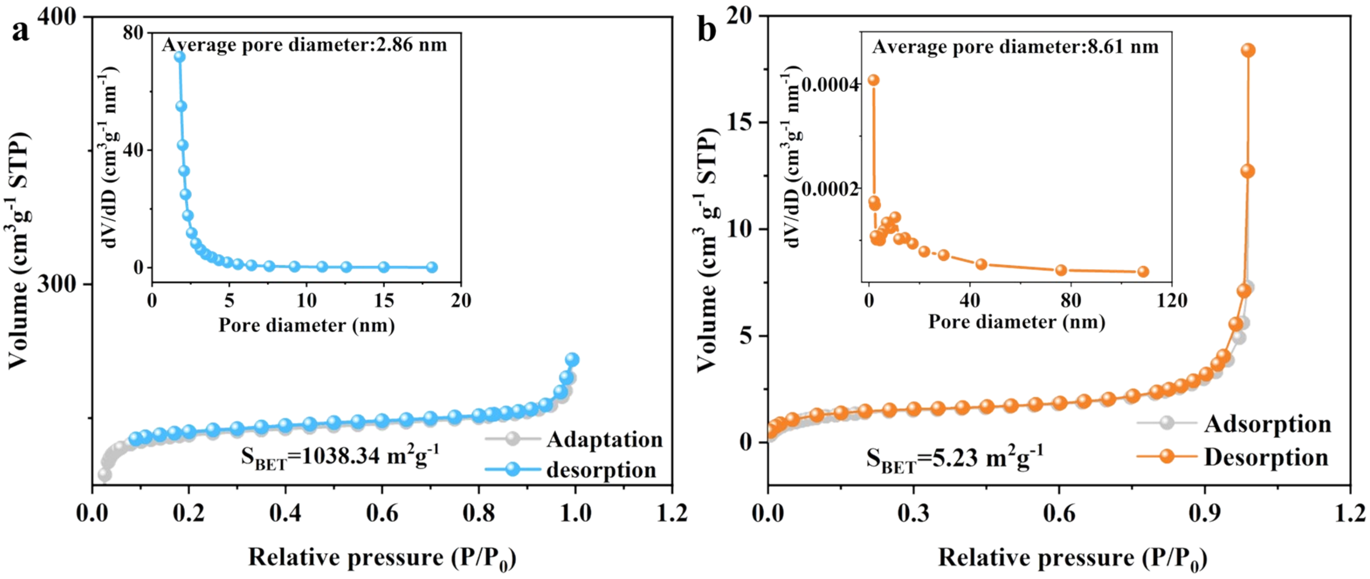

Fig. S2 N_2 adsorption-desorption isotherm and pore size distribution of (a) ZIF-8 and (b) PI nanofiber separators.

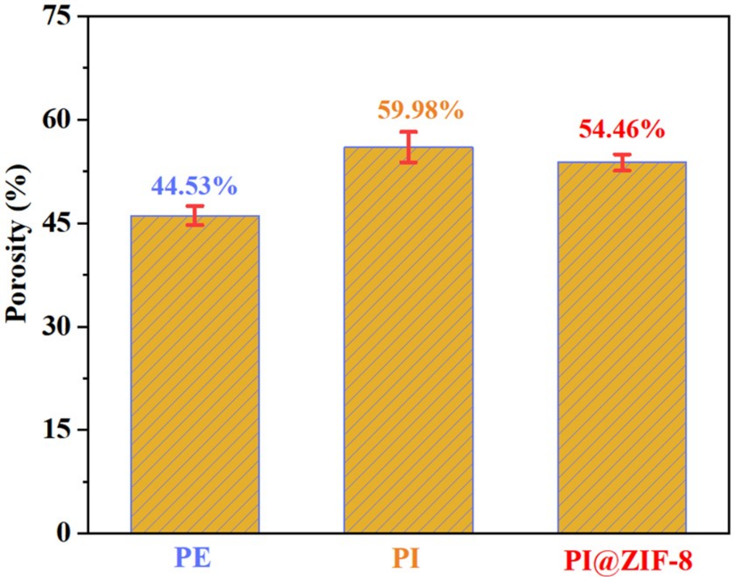

Fig. S3 The porosities of PE, PI and PI@ZIF-8 samples.

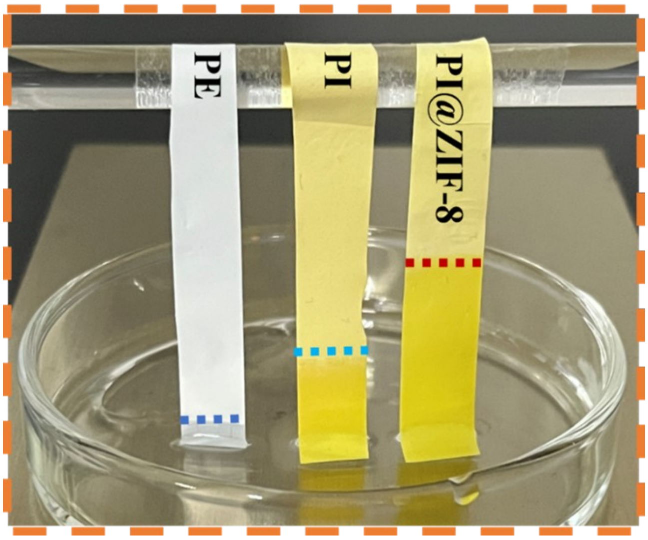

Fig. S4 Electrolyte immersion-heights of PE, PI and PI@ZIF-8 samples.

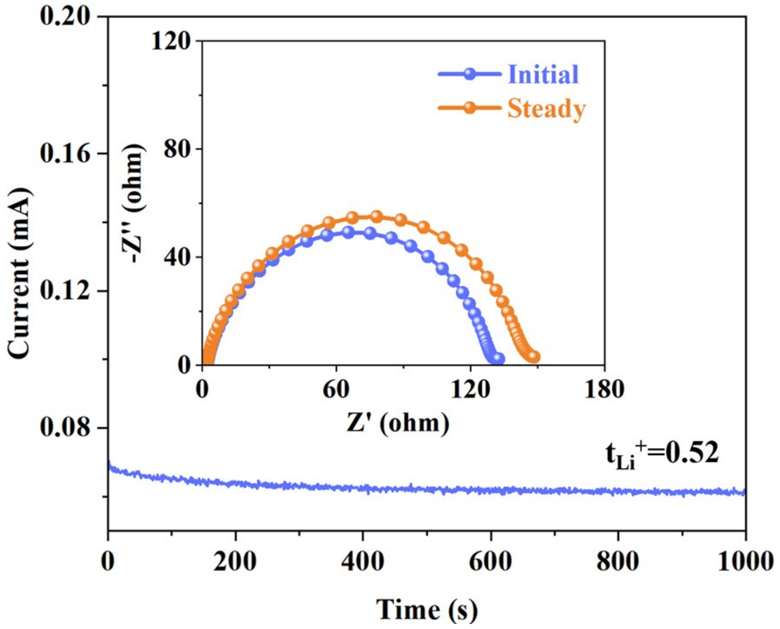

Fig. S5 Current-time curves and the relevant Nyquist plots of PE separators in symmetric Li‖Li cells.

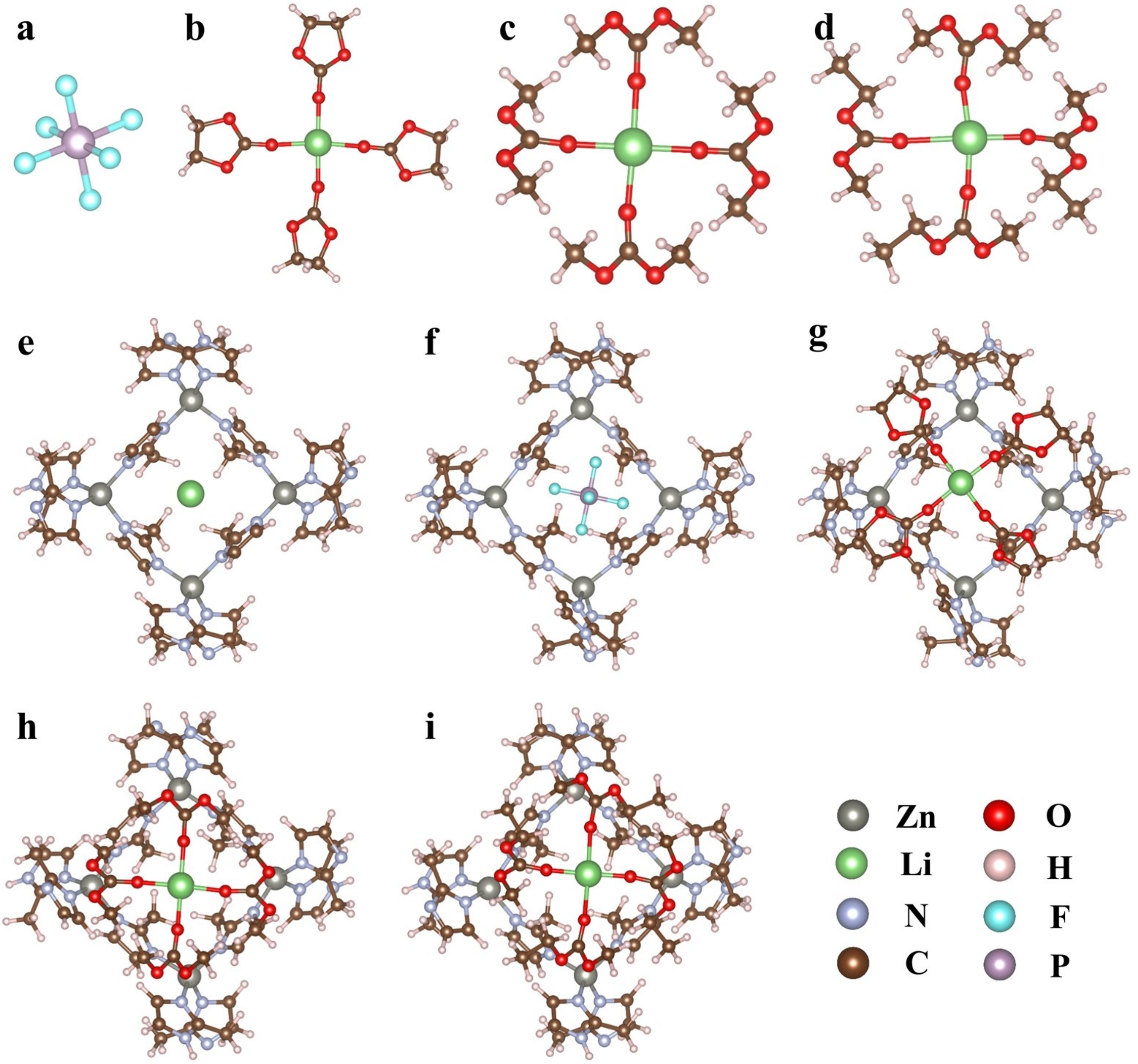

Fig. S6 Basic structures of electrolyte components of (a) PF_6^-, (b) $Li^+(EC)_4$, (c) $Li^+(DMC)_4$ and (d) $Li^+(EMC)_4$. Relaxed simulation models of 4-MR adsorbing (e) Li, (f) PF_6^-, (g) $Li^+(EC)_4$, (h) $Li^+(DMC)_4$ and (i) $Li^+(EMC)_4$.

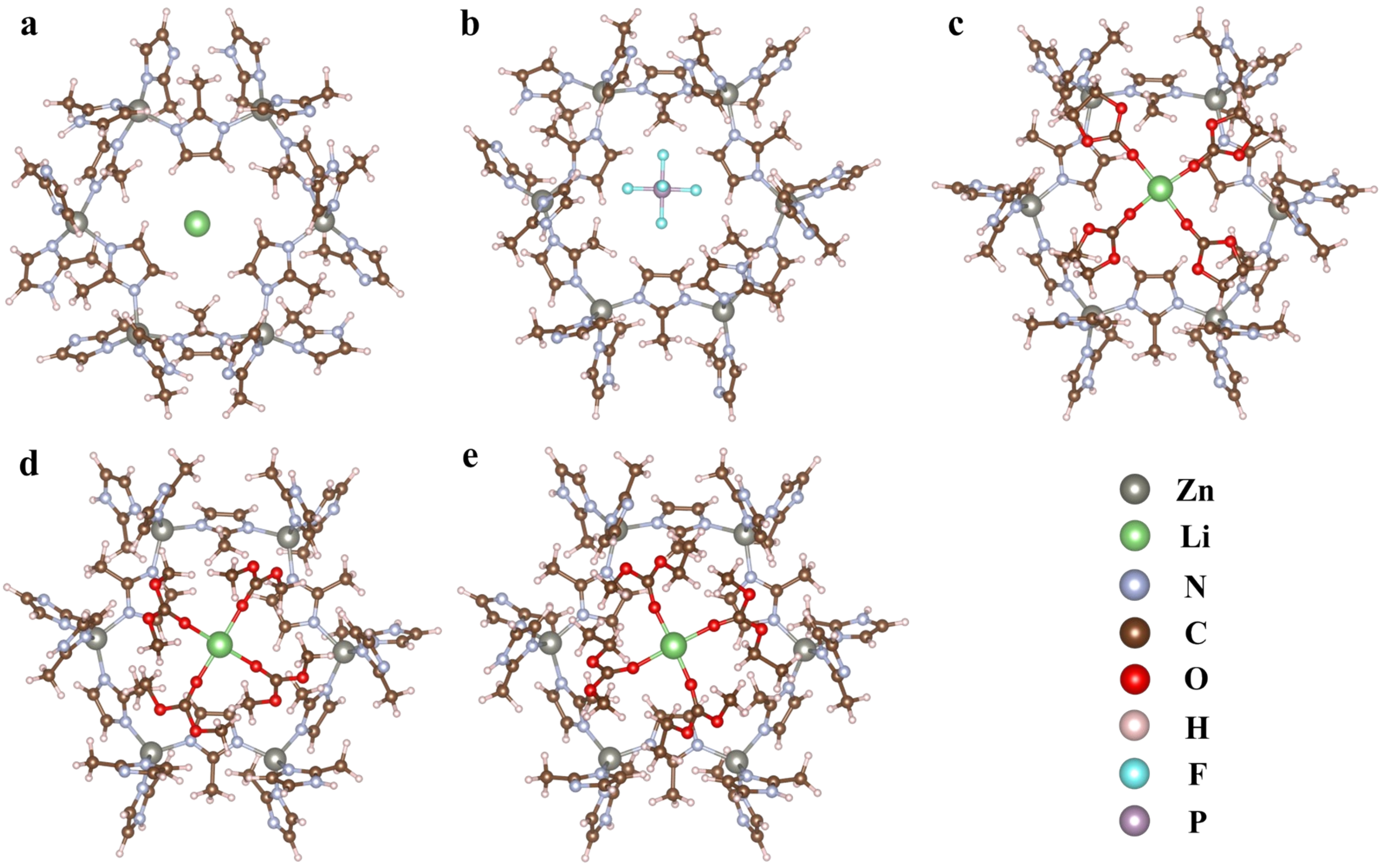

Fig. S7 Relaxed simulation models of 6-MR adsorbing (a) Li, (b) PF_6^-, (c) $Li^+(EC)_4$, (d) $Li^+(DMC)_4$ and (e) $Li^+(EMC)_4$.

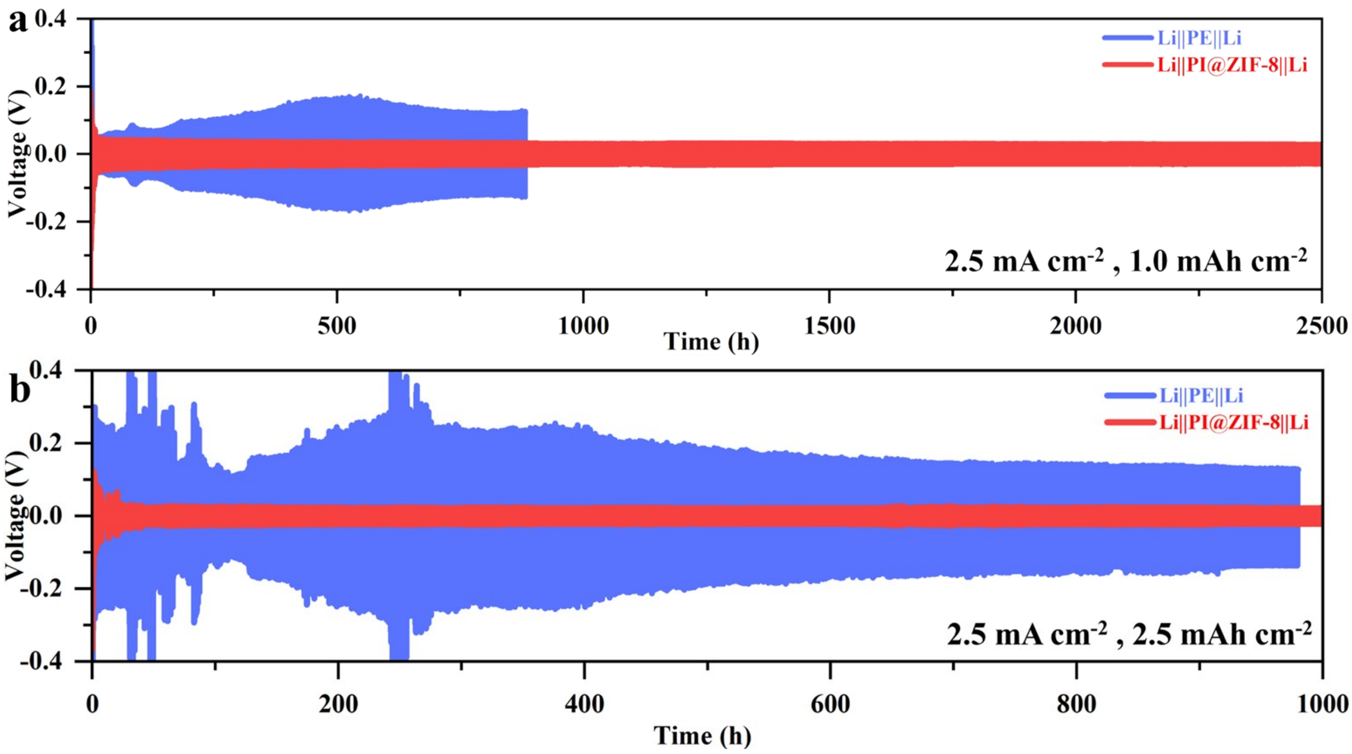

Fig. S8 Cycling performance of Li‖PE‖Li and Li‖PI@ZIF-8‖Li cells at (a) a current density of 2.5 mA cm^{-2} with an areal capacity of 1.0 mAh cm^{-2} and (b) a current density of 2.5 mA cm^{-2} with an areal capacity of 2.5 mAh cm^{-2}.

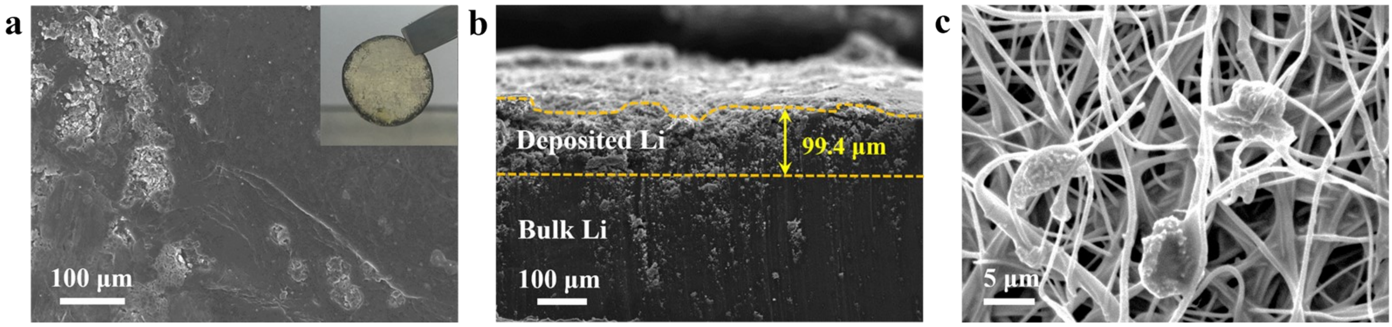

Fig. S9 Digital photograph and SEM images of the detached Li electrode and separator from the Li‖PI‖Li cells after cycling.

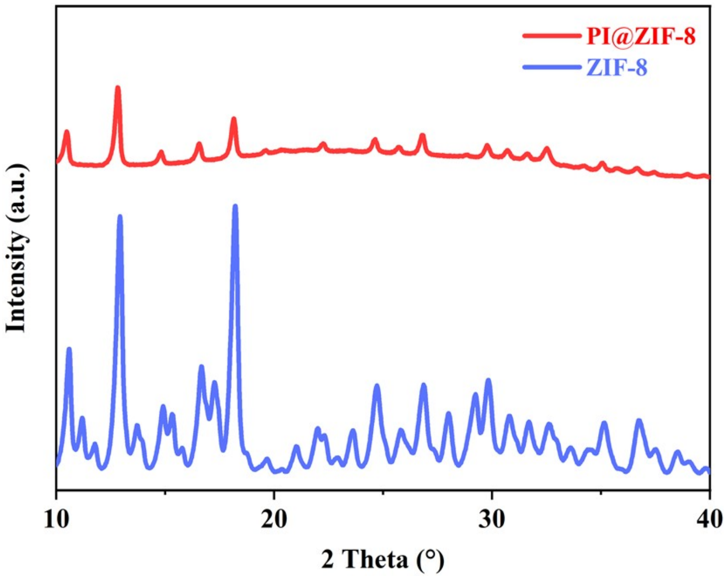

Fig. S10 XRD patterns of the PI@ZIF-8 nanofiber separators after cycling.

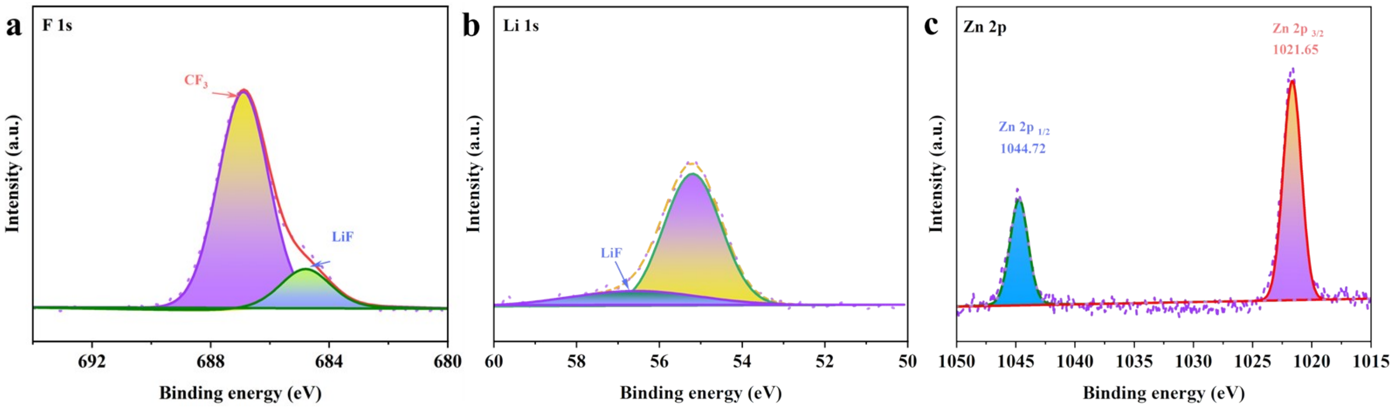

Fig. S11 The (a) F 1s and (b) Li 1s XPS spectra of the cycled Li anode surface. (c) Zn 2p XPS spectrum of the cycled PI@ZIF-8 separators.

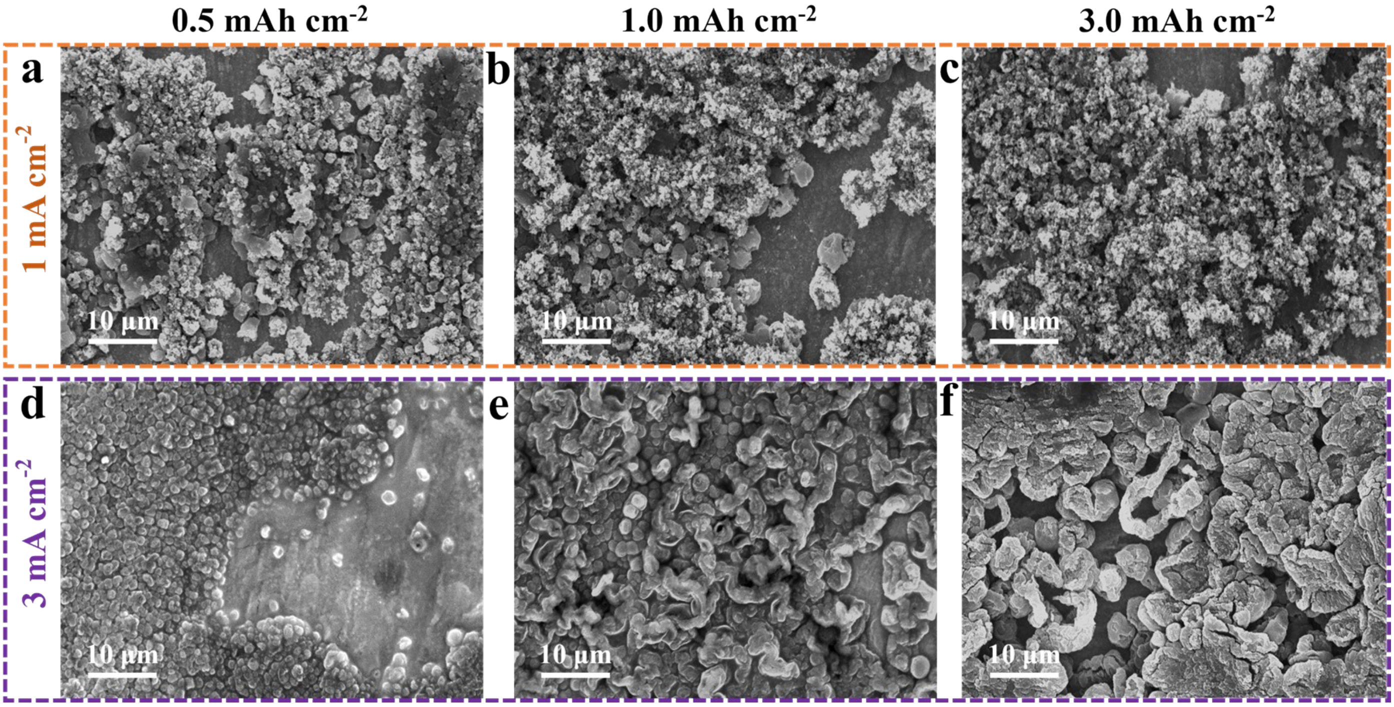

Fig. S12 SEM images of Li deposits on Cu foil within Li‖PE‖Cu cells discharged at (a-c) 1.0 mA cm^{-2} and (d-f) 3.0 mA cm^{-2} under different Li deposition amounts.

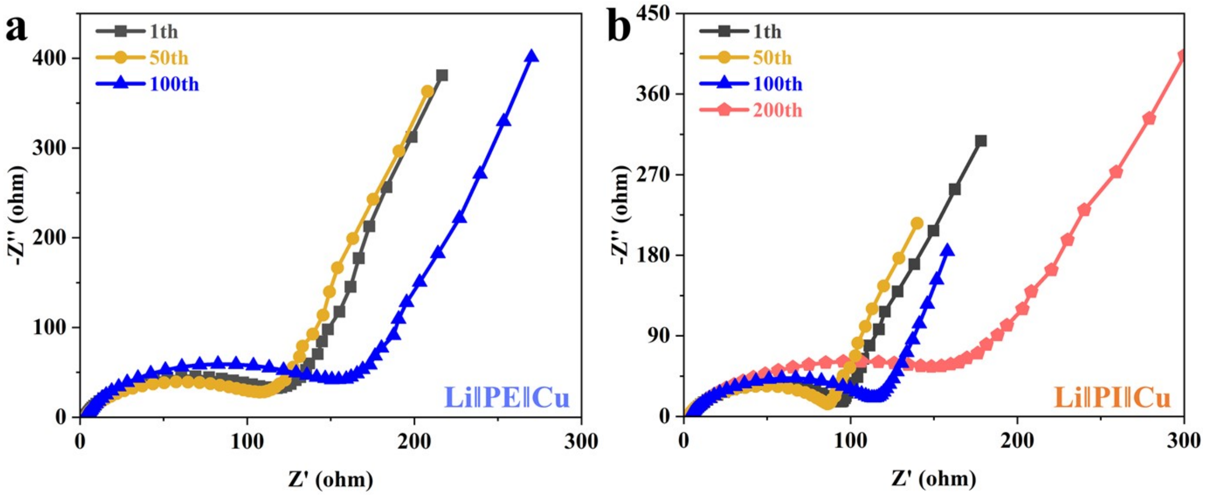

Fig. S13 Electrochemical impedances of (a) Li∥PE∥Cu and (b) Li∥PI∥Cu cells after cycling.

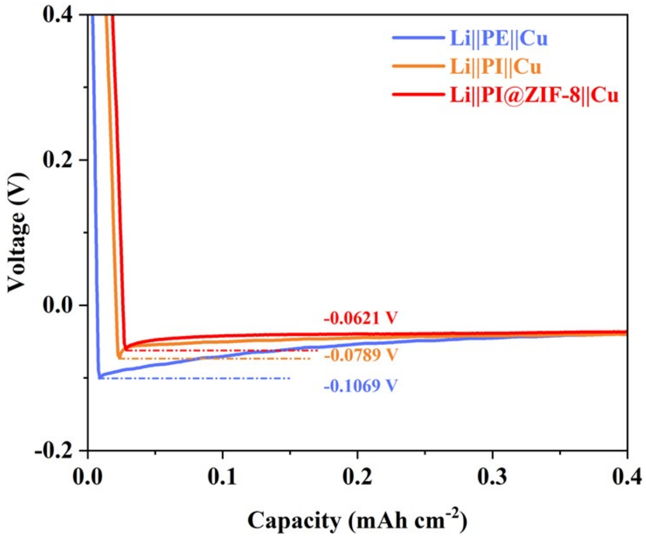

Fig. S14 Voltage-capacity curves of the initial Li deposition process for Li‖Cu cells.

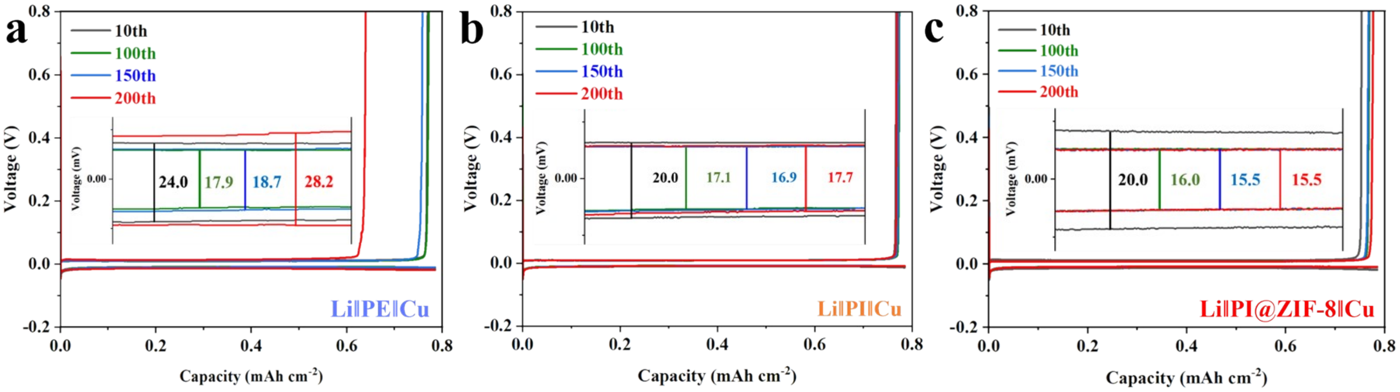

Fig. S15 The corresponding polarization profiles of (a) Li‖PE‖Cu, (b) Li‖PI‖Cu and (c) Li‖PI@ZIF-8‖Cu cells at different cycles.

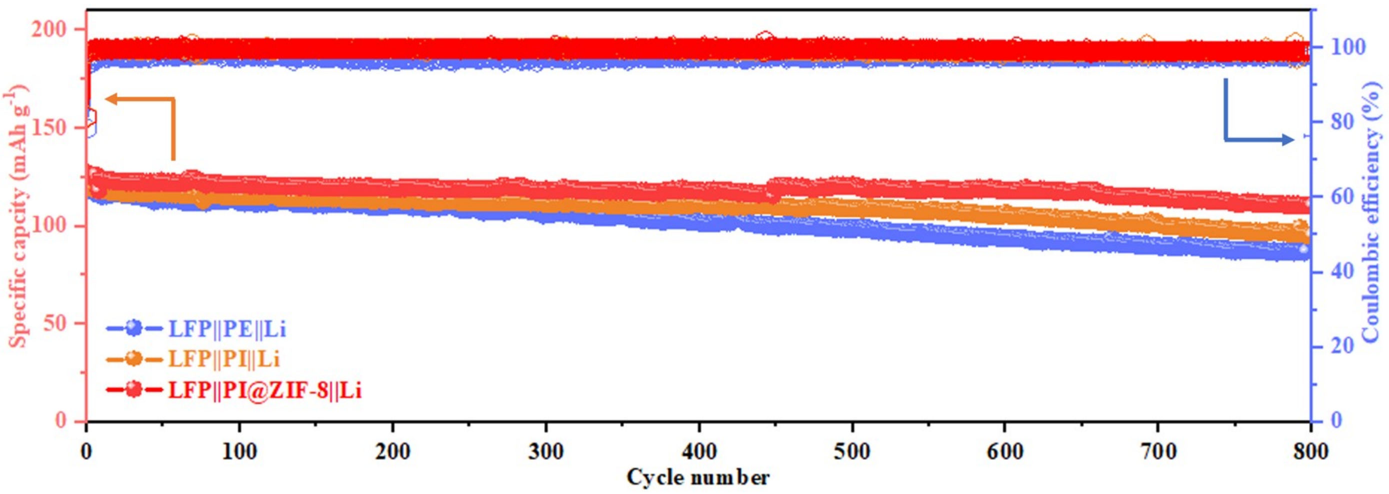

Fig. S16 Long-term cycle performance at 2.0 C of LFP‖PE‖Li, LFP‖PI‖Li and LFP‖PI@ZIF-8‖Li cells.

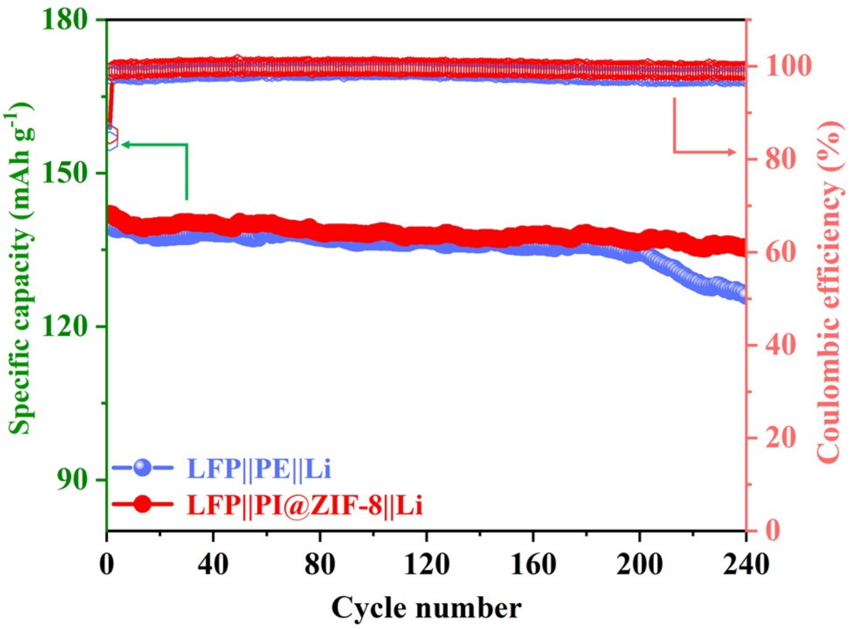

Fig. S17 Cycling performance of the assembled LFP‖Li cells with high-loading LFP cathodes at 1.0 C.

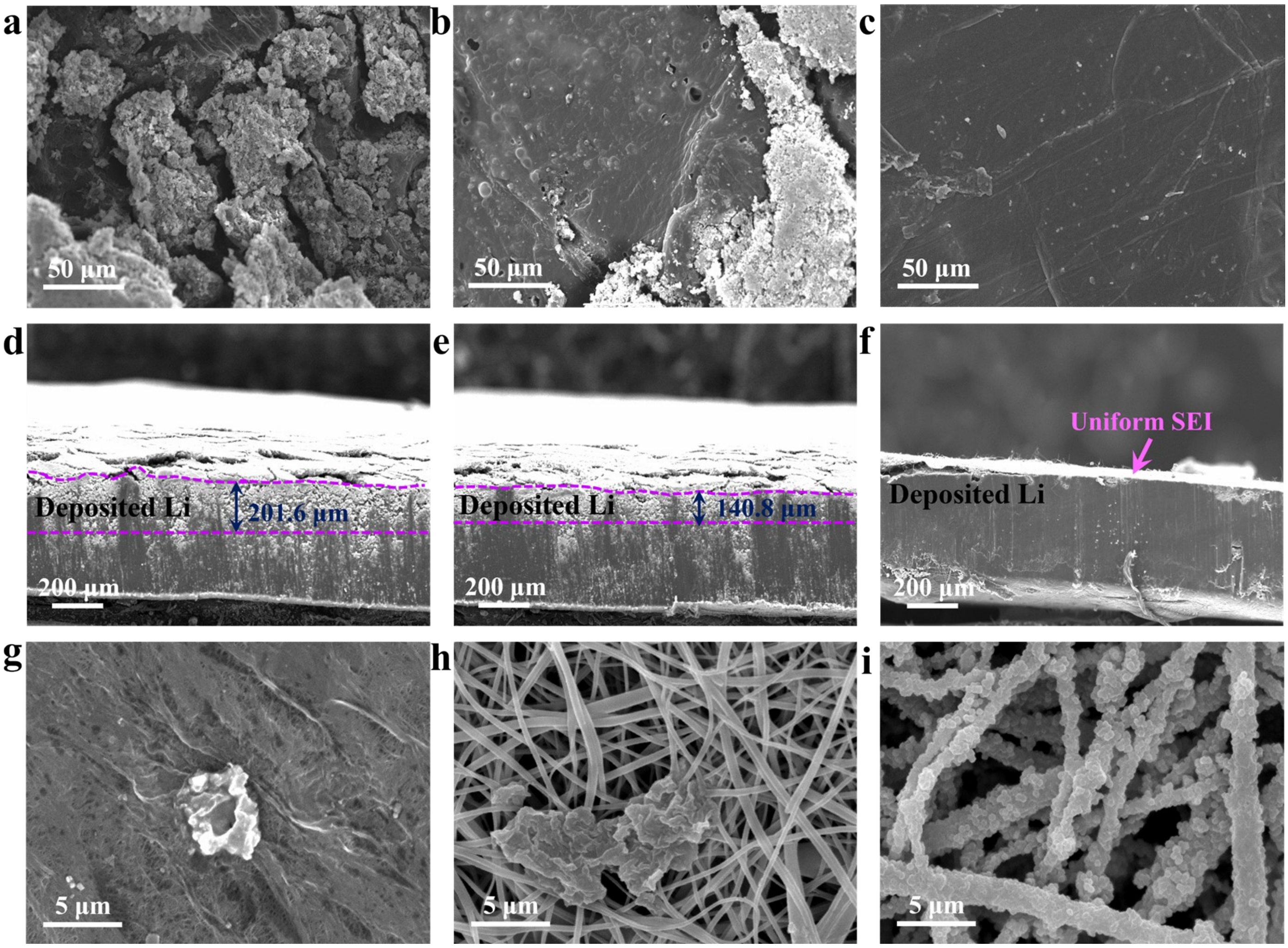

Fig. S18 SEM images of the detached Li anodes and separators from the (a, d, g) Li‖PE‖Li, (b, e, h) Li‖PI‖Li and (c, f, i) Li‖PI@ZIF-8‖Li cells after 300 cycles.

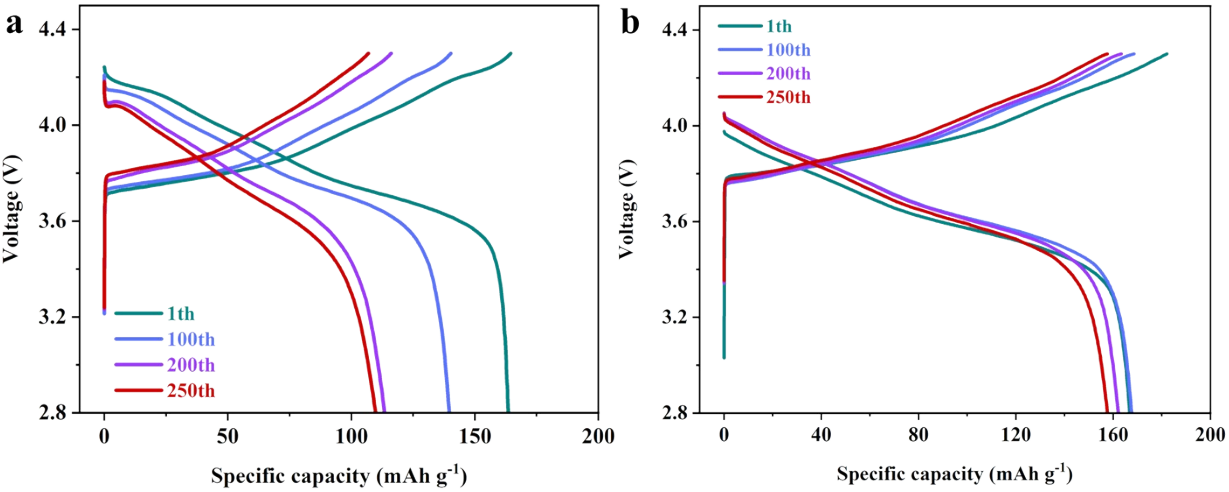

Fig. S19 Charge-discharge voltage profiles of (a) NCM811‖PE‖Li and NCM811‖PI@ZIF-8‖Li cells at different cycles.

Table S1 Thickness (h), bulk resistance (R_0) and ionic conductivity (σ) of the SS‖separator‖SS cells based on the three separators.

Samples	**h (μm)**	**R_0 (Ω)**	**σ (mS cm^{-1})**
PE	20	1.48	0.65
PI	49	1.43	1.65
PI@ZIF-8	47	0.94	2.40

Table S2 Comparison of the electrochemical performance for the Li-metal batteries using different nanofiber separators reported in the recent literatures.

Materials	**Ionic conductivity (mS cm^{-1})**	**Li$^+$ transference numbers**	**Cyclability (capacity retention after n cycles)**	**Ref.**
Cellulose/PI-COOH	0.51	/	90% after 200 cycles at 1.0 C	S1
PEI@PVDF-HFP	/	0.57	89.7% after 200 cycles at 0.2 C	S2
Triple cross-linking structured PI	3.9	/	44.9% after 500 cycles at 5.0 C	S3
ZnF$_2$-PCNFs	1.79	/	96.4% after 500 cycles at 1.0 C	S4
PI-OL@HNTs	1.86	0.86	92.1% after 300 cycles at 1.0 C	S5
ANFs/PEO	2.62	/	93.5% after 100 cycles at 2.0 C	S6
ZPBIA	1.62	0.57	86.4% after 500 cycles at 0.2 C	S7
PAN/cellulose	1.99	/	94.1% after 100 cycles at 0.5 C	S8
es-PVPSI	0.68	0.85	74.5% after 1000 cycles at 1.0 C	S9
PAN/AM-COF	3.30	0.79	85.5% after 400 cycles at 3.0 C	S10
PVDF/F-PI	1.05	/	80.3% after 1000 cycles at 2.0 C	S11
PMHP	2.79	/	87.6% after 100 cycles at 0.1 C	S12
PI@ZIF-8	**2.4**	**0.88**	**97.4% after 300 cycles at 1.0 C** **87.0% after 800 cycles at 2.0 C**	**This work**

References

S1 J. H. Deng, D. Q. Cao, X. Q. Yang and G. Q. Zhang, *Chem. Eng. J.*, 2022, **433**, 133934.

S2 Y. Zhang, R. H. He, Y. B. Li, H. Liu, H. H. Liu and X. X. Zhang, *Mater. Lett.*, 2024, **361**, 136063.

S3 Y. L. Chen, Z. L. Song, H. C. Liu, H. Xu, Y. C. Xi, C. Q. Yin, X. M. Li, L. Ma, P. X. Yan and L. Zhou, *ACS Sustain. Chem. Eng.*, 2024, **12**, 5953-5964.

S4 L. Y. Wei, N. P. Deng, J. G. Ju, H. J. Zhao, G. Wang, H. Y. Xiang, W. M. Kang and B. W. Cheng, *Chem. Eng. J.*, 2021, **424**, 130146.

S5 C. Y. Song, J. L. Luo, C. Gao, Q. G. Peng, M. E. Gibril, P. Fatehi, Z. G. Liu, S. J. Wang and F. G. Kong, *Int. J. Biol. Macromol.*, 2024, **273**, 132640.

S6 W. Tang, Q. Q. Liu, N. Luo, F. Chen and Q. Fu, *Compos. Sci. Technol.*, 2022, **225**, 109479.

S7 K. X. Gao, J. H. Luo, X. Li, K. Fan, L. B. Luo and X. Y. Liu, *J. Alloy. Compd.*, 2023, **996**, 171549.

S8 G. X. Dong, H. J. Li, Y. Wang, W. J. Jiang and Z. S. Ma, *Ionics*, 2021, **27**, 2955-2965.

S9 C. C. Li, B. S. Qin, Y. F. Zhang, A. Varzi, S. Passerini, J. Y. Wang, J. M. Dong, D. L. Zeng, Z. H. Liu and H. S. Cheng, *Adv. Energy Mater.*, 2019, **9**, 1803422.

S10 K. X. Wang, J. Duan, X. Chen, J. N. Wang, J. Q. Li, L. X. Jiang, W. Yan, W. Lyu and Y. Z. Liao, *Adv. Energy Mater.*, 2024, **14**, 2401146.

S11 Y. S. Qian, K. Chen, Z. X. Feng, Y. Ouyang, Q. Q. Lan, C. Zhang, W. Feng, Y. E. Miao and T. X. Liu, *Small Struct.*, 2023, **4**, 2200383.

S12 Y. K. Z.Yerkinbekova, S. Kalybekkyzy, N. Tolganbek, M. V. Kahraman, Z. Bakenov and A. Mentbayeva, *Sci Rep.*, 2022, **12**, 1827.